NASA/TM—2016-219391

Mechanical Model Development for Composite Structural Supercapacitors

Trenton M. Ricks and Thomas E. Lacy, Jr.
Mississippi State University, Mississippi State, Mississippi

Diana Santiago and Brett A. Bednarcyk
Glenn Research Center, Cleveland, Ohio

November 2016

NASA STI Program . . . in Profile

Since its founding, NASA has been dedicated to the advancement of aeronautics and space science. The NASA Scientific and Technical Information (STI) Program plays a key part in helping NASA maintain this important role.

The NASA STI Program operates under the auspices of the Agency Chief Information Officer. It collects, organizes, provides for archiving, and disseminates NASA's STI. The NASA STI Program provides access to the NASA Technical Report Server—Registered (NTRS Reg) and NASA Technical Report Server—Public (NTRS) thus providing one of the largest collections of aeronautical and space science STI in the world. Results are published in both non-NASA channels and by NASA in the NASA STI Report Series, which includes the following report types:

- TECHNICAL PUBLICATION. Reports of completed research or a major significant phase of research that present the results of NASA programs and include extensive data or theoretical analysis. Includes compilations of significant scientific and technical data and information deemed to be of continuing reference value. NASA counter-part of peer-reviewed formal professional papers, but has less stringent limitations on manuscript length and extent of graphic presentations.

- TECHNICAL MEMORANDUM. Scientific and technical findings that are preliminary or of specialized interest, e.g., "quick-release" reports, working papers, and bibliographies that contain minimal annotation. Does not contain extensive analysis.

- CONTRACTOR REPORT. Scientific and technical findings by NASA-sponsored contractors and grantees.

- CONFERENCE PUBLICATION. Collected papers from scientific and technical conferences, symposia, seminars, or other meetings sponsored or co-sponsored by NASA.

- SPECIAL PUBLICATION. Scientific, technical, or historical information from NASA programs, projects, and missions, often concerned with subjects having substantial public interest.

- TECHNICAL TRANSLATION. English-language translations of foreign scientific and technical material pertinent to NASA's mission.

For more information about the NASA STI program, see the following:

- Access the NASA STI program home page at http://www.sti.nasa.gov

- E-mail your question to help@sti.nasa.gov

- Fax your question to the NASA STI Information Desk at 757-864-6500

- Telephone the NASA STI Information Desk at 757-864-9658

- Write to:
  NASA STI Program
  Mail Stop 148
  NASA Langley Research Center
  Hampton, VA 23681-2199

NASA/TM—2016-219391

Mechanical Model Development for Composite Structural Supercapacitors

Trenton M. Ricks and Thomas E. Lacy, Jr.
Mississippi State University, Mississippi State, Mississippi

Diana Santiago and Brett A. Bednarcyk
Glenn Research Center, Cleveland, Ohio

National Aeronautics and
Space Administration

Glenn Research Center
Cleveland, Ohio 44135

November 2016

Acknowledgments

This work was sponsored by the NASA Aeronautics Research Mission Directorate, Transformative Aeronautics Concepts Program, Convergent Aeronautics Solutions Project, Multifunctional Structures for High Energy Lightweight Load-Bearing Storage (M–SHELLS) Project.

Level of Review: This material has been technically reviewed by technical management.

Available from

NASA STI Program
Mail Stop 148
NASA Langley Research Center
Hampton, VA 23681-2199

National Technical Information Service
5285 Port Royal Road
Springfield, VA 22161
703-605-6000

This report is available in electronic form at http://www.sti.nasa.gov/ and http://ntrs.nasa.gov/

Mechanical Model Development for Composite Structural Supercapacitors

Trenton M. Ricks and Thomas E. Lacy, Jr.
Mississippi State University
Mississippi State, Mississippi 39762

Diana Santiago and Brett A. Bednarcyk
National Aeronautics and Space Administration
Glenn Research Center
Cleveland, Ohio 44135

Abstract

Novel composite structural supercapacitor concepts have recently been developed as a means both to store electrical charge and to provide modest mechanical load carrying capability. Double-layer composite supercapacitors are often fabricated by impregnating a woven carbon fiber fabric, which serves as the electrodes, with a structural polymer electrolyte. Polypropylene or a glass fabric is often used as the separator material. Recent research has been primarily limited to evaluating these composites experimentally. In this study, mechanical models based on the Multiscale Generalized Method of Cells (MSGMC) were developed and used to calculate the shear and tensile properties and response of two composite structural supercapacitors from the literature. The modeling approach was first validated against traditional composite laminate data. MSGMC models for composite supercapacitors were developed, and accurate elastic shear/tensile properties were obtained. It is envisioned that further development of the models presented in this work will facilitate the design of composite components for aerospace and automotive applications and can be used to screen candidate constituent materials for inclusion in future composite structural supercapacitor concepts.

Introduction

Multifunctional composite structural supercapacitors have recently emerged as a means of storing electrical charge while withstanding mechanical loads. As shown in Figure 1, traditional supercapacitors represent a compromise between batteries (high energy density, moderate power density) and dielectric capacitors (low energy density, high power density). Conventional supercapacitors have energy and power densities of approximately 3-10 $Whkg^{-1}$ and 3 $kWkg^{-1}$, respectively (Ref. 1). Similar to batteries, double-layer supercapacitors are comprised of three main components: the electrodes, an electrolyte, and a separator material. During charging or discharging processes, ions are conducted from one electrode to another through the electrolyte. The two electrodes are separated by a porous separator material that is electrically insulating but allows ion flow. For composite structural supercapacitors, woven carbon fabric (CF) is often the electrode material. CFs are commonly chemically activated or modified in order to obtain better electrical properties (Ref. 1). A solid polymer electrolyte (SPE) is used as the primary means to conduct ions from one electrode to the other. Although SPEs have an ionic conductivity several orders of magnitude lower than liquid electrolytes, SPEs are required in composite structural supercapacitors to serve as the matrix in order for the structure to carry any significant mechanical loads (Ref. 1). A porous polypropylene (PP) membrane or glass fabric is commonly used as the separator material. The separator material and thickness should be carefully selected since PP membranes have been observed to promote delamination in composite supercapacitors upon mechanical loading, (Ref. 2) and supercapacitors with a glass fabric separator can be prone to shorting (i.e., loss of the ability to store a charge) (Refs. 3 and 4).

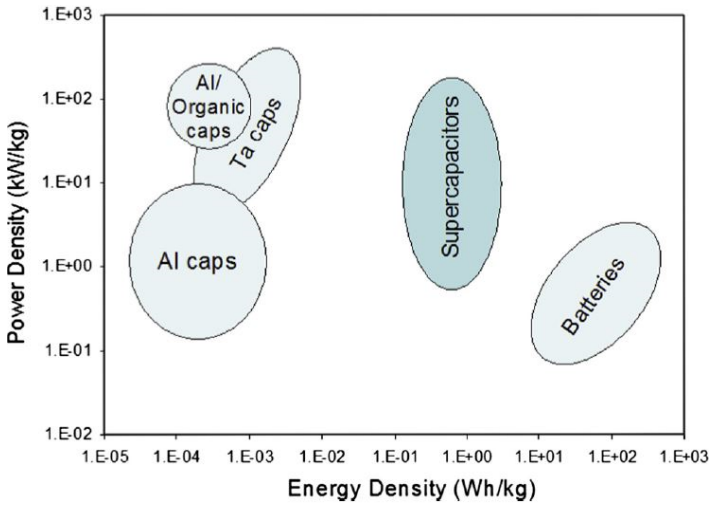

Figure 1.—Relationship between power and energy density for capacitors, supercapacitors, and batteries (figure from Ref. 1).

Recent research in this area has been primarily limited to experimental testing. In order to facilitate the use of composite supercapacitors into structural aerospace and automotive components, mechanical and electrochemical modeling and design strategies must be established. In this study, micromechanics-based mechanical models are developed and used to calculate the mechanical response of two composite structural supercapacitor concepts that have been recently reported in the literature.

Modeling Approach

The Multiscale Generalized Method of Cells (MSGMC)

The Generalized Method of Cells (GMC) micromechanics theory is an efficient, semi-analytical method that provides the homogenized, nonlinear constitutive response of a composite material. Its foundations for single scale analysis, along with validation of its results, are well-established in the literature (c.f., Ref. 6). The GMC method considers the composite microstructure, on a given length scale, to be periodic, with a repeating unit cell (RUC) as shown (at a given length scale) in Figure 2. The unit cell is discretized into N_α by N_β by N_γ subcells, each of which may contain a distinct material. However, as indicated in Figure 2, the unique feature of MSGMC is that the materials occupying the subcells on a given length scale may themselves be heterogeneous composite materials, represented by a unique RUC. A given analysis may consist of k arbitrary explicit length scales (see Fig. 2). The highest length scale considered is denoted as Level 0, whereas, the current length scale under consideration is length scale *i, where i = 0,1,…,k.*

The GMC theory assumes a first-order displacement field in the subcells at a given scale, resulting in constant stresses and strains per subcell (Ref. 6). Assuming infinitesimal strains, the constitutive equation for the subcells at Level i is given by,

$$\boldsymbol{\sigma}_i^{(\alpha_i\beta_i\gamma_i)} = \mathbf{C}_i^{(\alpha_i\beta_i\gamma_i)}\left(\boldsymbol{\varepsilon}_i^{(\alpha_i\beta_i\gamma_i)} - \boldsymbol{\varepsilon}_i^{I(\alpha_i\beta_i\gamma_i)}\right) \tag{1}$$

where $\boldsymbol{\sigma}_i$ is the stress tensor, $\mathbf{C}_i$ is the stiffness tensor, $\boldsymbol{\varepsilon}_i$ is the total strain tensor, and $\boldsymbol{\varepsilon}_i^I$ is the inelastic strain tensor for the i^{th} Level. The superscript $(\alpha_i\,\beta_i\,\gamma_i)$ denotes the particular subcell at Level i. Note that thermal strains are not considered herein.

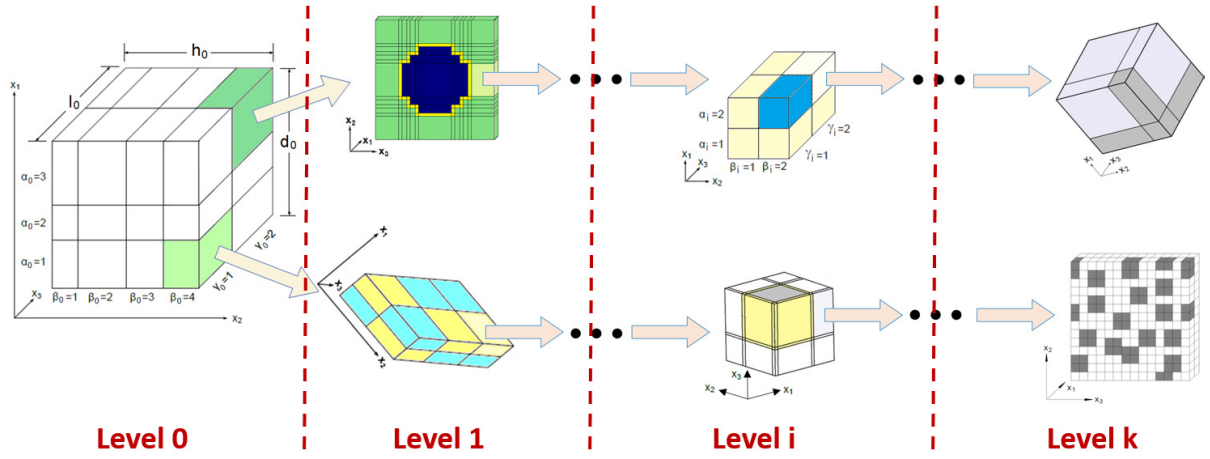

Figure 2.—MSGMC repeating unit cells (RUCs) and subcells across an arbitrary number of length scales.

Satisfaction of displacement and traction continuity between subcells in an average (integral) sense, and imposition of periodicity conditions along the RUC boundaries enable the establishment of a system of linear algebraic equations, which can be solved to determine the elastic and inelastic strain concentration matrices, $\mathbf{A}_i^{(\alpha_i\beta_i\gamma_i)}$ and $\mathbf{D}_i^{(\alpha_i\beta_i\gamma_i)}$, respectively. The reader is referred to Aboudi et al. (Ref. 6) for more details regarding this formulation. At a given Level of scale, *i*, these concentration tensors characterize the local strain tensors in the subcells in terms of the RUC-averaged total strain tensor, $\overline{\boldsymbol{\varepsilon}}_i$ and the (properly arranged) matrix of inelastic strains in all subcells, $\boldsymbol{\varepsilon}_{\mathbf{S}i}^I$,

$$\boldsymbol{\varepsilon}_i^{(\alpha_i\beta_i\gamma_i)} = \mathbf{A}_i^{(\alpha_i\beta_i\gamma_i)}\overline{\boldsymbol{\varepsilon}}_i + \mathbf{D}_i^{(\alpha_i\beta_i\gamma_i)}\boldsymbol{\varepsilon}_{\mathbf{S}i}^I \tag{2}$$

In the multiscale analysis, all terms in Equation (2) depend on the location of the Level *i* RUC within all higher scale RUCs. In essence, the strain in a given subcell at Level *k* depends on the path taken down the length scales from Level 0. Equation (1) can be recast in terms of average strains by substituting Equation (2) into Equation (1),

$$\boldsymbol{\sigma}_i^{(\alpha_i\beta_i\gamma_i)} = \mathbf{C}_i^{(\alpha_i\beta_i\gamma_i)}\left(\mathbf{A}_i^{(\alpha_i\beta_i\gamma_i)}\overline{\boldsymbol{\varepsilon}}_i + \mathbf{D}_i^{(\alpha_i\beta_i\gamma_i)}\boldsymbol{\varepsilon}_{\mathbf{S}i}^I - \boldsymbol{\varepsilon}_i^{I(\alpha_i\beta_i\gamma_i)}\right) \tag{3}$$

The RUC-averaged stress tensor is given by,

$$\overline{\boldsymbol{\sigma}}_i = \frac{1}{d_i h_i l_i}\sum_{\alpha_i=1}^{N_{\alpha_i}}\sum_{\beta_i=1}^{N_{\beta_i}}\sum_{\gamma_i=1}^{N_{\gamma_i}} d_{\alpha_i} h_{\beta_i} l_{\gamma_i}\boldsymbol{\sigma}_i^{(\alpha_i\beta_i\gamma_i)} \tag{4}$$

where d_{α_i}, h_{β_i}, l_{γ_i} are the dimensions of subcell $(\alpha_i\beta_i\gamma_i)$ and d_i, h_i, l_i are the RUC dimensions for Level *i*. Equations (3) and (4) lead to,

$$\overline{\boldsymbol{\sigma}}_i = \frac{1}{d_i h_i l_i}\sum_{\alpha_i=1}^{N_{\alpha_i}}\sum_{\beta_i=1}^{N_{\beta_i}}\sum_{\gamma_i=1}^{N_{\gamma_i}} d_{\alpha_i} h_{\beta_i} l_{\gamma_i}\mathbf{C}_i^{(\alpha_i\beta_i\gamma_i)}\left(\mathbf{A}_i^{(\alpha_i\beta_i\gamma_i)}\overline{\boldsymbol{\varepsilon}}_i + \mathbf{D}_i^{(\alpha_i\beta_i\gamma_i)}\boldsymbol{\varepsilon}_{\mathbf{S}i}^I - \boldsymbol{\varepsilon}_i^{I(\alpha_i\beta_i\gamma_i)}\right) \tag{5}$$

The effective constitutive equation at Level *i* is given by,

$$\overline{\boldsymbol{\sigma}}_i = \mathbf{C}_i^* \left(\overline{\boldsymbol{\varepsilon}}_i - \overline{\boldsymbol{\varepsilon}}_i^I \right) \tag{6}$$

where $\overline{\boldsymbol{\varepsilon}}_i^I$ is the RUC-averaged inelastic strain tensor. Equations (5) and (6) indicate that the effective stiffness tensor, $\mathbf{C}_i^*$, at Level *i* is given by,

$$\mathbf{C}_i^* = \frac{1}{d_i h_i l_i} \sum_{\alpha_i=1}^{N_{\alpha_i}} \sum_{\beta_i=1}^{N_{\beta_i}} \sum_{\gamma_i=1}^{N_{\gamma_i}} d_{\alpha_i} h_{\beta_i} l_{\gamma_i} \mathbf{C}_i^{(\alpha_i\beta_i\gamma_i)} \mathbf{A}_i^{(\alpha_i\beta_i\gamma_i)} \tag{7}$$

Similarly, $\overline{\boldsymbol{\varepsilon}}_i^I$ is given by,

$$\overline{\boldsymbol{\varepsilon}}_i^I = \frac{-\mathbf{C}_i^{*-1}}{d_i h_i l_i} \sum_{\alpha_i=1}^{N_{\alpha_i}} \sum_{\beta_i=1}^{N_{\beta_i}} \sum_{\gamma_i=1}^{N_{\gamma_i}} d_{\alpha_i} h_{\beta_i} l_{\gamma_i} \mathbf{C}_i^{(\alpha_i\beta_i\gamma_i)} \left(\mathbf{D}_i^{(\alpha_i\beta_i\gamma_i)} \boldsymbol{\varepsilon}_{\mathbf{S}i}^I - \boldsymbol{\varepsilon}_i^{I(\alpha_i\beta_i\gamma_i)} \right) \tag{8}$$

In MSGMC, the scales are linked by considering the RUC-averaged stress, total strain, inelastic strain, and stiffness tensors at scale *i* to be equal to the local subcell stress, strain, and stiffness tensors of the applicable subcell from the next higher length scale (*i*-1). An appropriate coordinate transformation is used to account for the potential coordinate system change from scale to scale. That is,

$$\overline{\boldsymbol{\varepsilon}}_i = \mathbf{T}_2^i \, \boldsymbol{\varepsilon}_{i-1}^{(\alpha_{i-1}\beta_{i-1}\gamma_{i-1})}, \; \overline{\boldsymbol{\varepsilon}}_i^I = \mathbf{T}_2^i \, \boldsymbol{\varepsilon}_{i-1}^{I(\alpha_{i-1}\beta_{i-1}\gamma_{i-1})}, \; \overline{\boldsymbol{\sigma}}_i = \mathbf{T}_2^i \, \boldsymbol{\sigma}_{i-1}^{(\alpha_{i-1}\beta_{i-1}\gamma_{i-1})}, \; \mathbf{C}_i^* = \mathbf{T}_4^i \, \mathbf{C}_{i-1}^{(\alpha_{i-1}\beta_{i-1}\gamma_{i-1})}, i = 1, \ldots, k \tag{9}$$

where $\mathbf{T}_2^i$ and $\mathbf{T}_4^i$ are the appropriate second and fourth order coordinate transformation tensors, respectively. Hence, it is clear that, starting with the lowest scale (*k*) RUC (see Fig. 2), whose subcells contain only monolithic materials, the effective stiffness tensor can be calculated using the standard GMC method. This stiffness tensor (after appropriate coordinate transformation) then represents the homogenized material in one of the subcells within an RUC at the next higher length scale (*k*-1). Given the transformed effective stiffness tensors of all subcells at the successively higher length scale, the effective stiffness tensor of the RUC at this Level can be determined. This stiffness tensor can then be transformed and passed along to the next higher length scale in a similar fashion, and the process repeats until the highest length scale considered (*i* = 0) is reached.

As an example, for an MSGMC analysis considering three length scales (*i* = 0, 1, and 2), the overall effective stiffness tensor can be written using Equations (7), (9) as,

$$\mathbf{C}_0^* = \frac{1}{d_0 h_0 l_0} \sum_{\alpha_0\beta_0\gamma_0} d_{\alpha_0} h_{\beta_0} l_{\gamma_0} \left\{ \frac{\left(\mathbf{T}_4^1\right)^{-1}}{d_1 h_1 l_1} \sum_{\alpha_1\beta_1\gamma_1} d_{\alpha_1} h_{\beta_1} l_{\gamma_1} \left[\frac{\left(\mathbf{T}_4^2\right)^{-1}}{d_2 h_2 l_2} \sum_{\alpha_2\beta_2\gamma_2} d_{\alpha_2} h_{\beta_2} l_{\gamma_2} \mathbf{C}_2^{(\alpha_2\beta_2\gamma_2)} \mathbf{A}_2^{(\alpha_2\beta_2\gamma_2)} \right]^{(\alpha_1\beta_1\gamma_1)} \mathbf{A}_1^{(\alpha_1\beta_1\gamma_1)} \right\}^{(\alpha_0\beta_0\gamma_0)} \mathbf{A}_0^{(\alpha_0\beta_0\gamma_0)} \tag{10}$$

where a contracted notation has been used for the triple summation at each scale. Note that, in Equation (9), the superscript on the bracketed terms indicates that all variables within the brackets are a function of the subcell indices from the next higher length scale (including lower scale dimensions and subcell indices). The intent of this notation is to fully define the location of a subcell at a given scale as one progresses down the length scales. For example, using this notation, the effective stiffness tensor at Level 2, from Equation (9) can be written as,

$$\left\{ \left[\mathbf{C}_2^* \right]^{(\alpha_1\beta_1\gamma_1)} \right\}^{(\alpha_0\beta_0\gamma_0)} = \left\{ \left[\mathbf{T}_4^2 \right]^{(\alpha_1\beta_1\gamma_1)} \right\}^{(\alpha_0\beta_0\gamma_0)} \left\{ \mathbf{C}_1^{(\alpha_1\beta_1\gamma_1)} \right\}^{(\alpha_0\beta_0\gamma_0)} \tag{11}$$

as there are distinct $\mathbf{C}_2^*$ values for every Level 1 subcell, while there are distinct Level 1 RUCs present within each Level 0 subcell.

Alternatively, MSGMC can perform multiscale *localization* of the stress and strain tensors. For the three length scale example, the local total strain tensor in an arbitrary lowest scale ($k = 2$) subcell can be written using Equations (2), (9) as,

$$\left\{ \left[\boldsymbol{\varepsilon}_2^{(\alpha_2\beta_2\gamma_2)} \right]^{(\alpha_1\beta_1\gamma_1)} \right\}^{(\alpha_0\beta_0\gamma_0)} = \left\{ \left[\mathbf{A}_2^{(\alpha_2\beta_2\gamma_2)} \overline{\boldsymbol{\varepsilon}}_2^{(\alpha_2\beta_2\gamma_2)} + \mathbf{D}_2^{(\alpha_2\beta_2\gamma_2)} \boldsymbol{\varepsilon}_{\mathbf{S}2}^{I(\alpha_2\beta_2\gamma_2)} \right]^{(\alpha_1\beta_1\gamma_1)} \right\}^{(\alpha_0\beta_0\gamma_0)} \tag{12}$$

$$\overline{\boldsymbol{\varepsilon}}_2^{(\alpha_2\beta_2\gamma_2)} = \left\{ \left[\mathbf{T}_2^2 \right]^{(\alpha_1\beta_1\gamma_1)} \right\}^{(\alpha_0\beta_0\gamma_0)} \left\{ \mathbf{A}_1^{(\alpha_1\beta_1\gamma_1)} \overline{\boldsymbol{\varepsilon}}_1^{(\alpha_1\beta_1\gamma_1)} + \mathbf{D}_1^{(\alpha_1\beta_1\gamma_1)} \boldsymbol{\varepsilon}_{\mathbf{S}1}^{I(\alpha_2\beta_2\gamma_2)} \right\}^{(\alpha_0\beta_0\gamma_0)} \tag{13}$$

$$\overline{\boldsymbol{\varepsilon}}_1^{(\alpha_1\beta_1\gamma_1)} = \left\{ \mathbf{T}_2^1 \right\}^{(\alpha_0\beta_0\gamma_0)} \left(\mathbf{A}_0^{(\alpha_0\beta_0\gamma_0)} \overline{\boldsymbol{\varepsilon}}_0 + \mathbf{D}_0^{(\alpha_0\beta_0\gamma_0)} \boldsymbol{\varepsilon}_{\mathbf{S}0}^{I} \right) \tag{14}$$

Again, the superscript on the bracketed terms indicates that all variables within the brackets are a function of the subcell indices from the next higher length scale (including subcell indices). The subcell inelastic strains at any length scale, $\boldsymbol{\varepsilon}_{S_i}^I$, are obtained from the lower length scale inelastic strains, along with appropriate transformations (see Eqs. (8) and (9)). The stress tensor for any subcell at any length scale can be similarly determined through localization, or by simply using the strain tensor, along with the constitutive equation, at the appropriate length scale.

Modeling of Composite Structural Supercapacitors

MSGMC was used to simulate the mechanical behavior (shear/tensile) of double-layer composite supercapacitors. As previously mentioned, most reported composite structural supercapacitor concepts are comprised of woven CF (often plain weave) electrodes. Consequently, although general weaves can be analyzed with MSGMC, only plain weave CF electrodes were considered in this study. Using this approach, key geometric features of a woven fabric architecture were represented using a triply-periodic RUC. An idealized representation of a plain weave fabric composite is shown in Figure 3. Each subcell was used to approximate the homogenized fiber tow/matrix or the matrix only for a plain weave geometry.

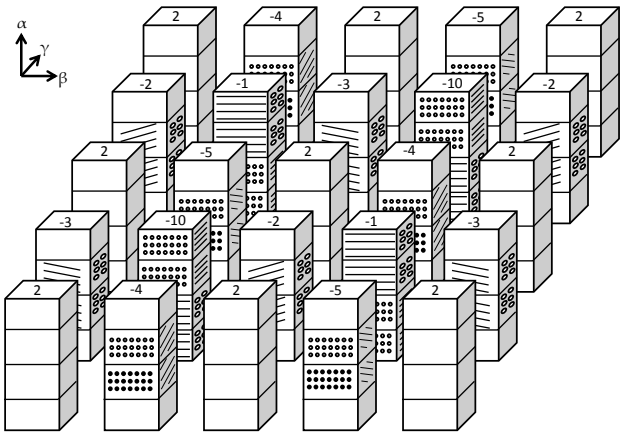

Figure 3.—MSGMC plain weave fabric representation (k = 2). Note that negative numbers indicate distinct "stacks" of subcells specific to the internal MAC/GMC library while a positive two indicates a stack of matrix only subcells.

The fiber tow is represented by its own triply periodic RUC based on a user-specified fiber tow volume fraction and packing configuration. By simulating a woven fabric in this manner, the ply, tow, and intertow geometry can be idealized to accurately simulate a composite ply. The mechanical response of both the global and tow RUCs was determined using the triply-periodic generalized method of cells (Ref. 6). A two-step homogenization procedure was used to determine the effective mechanical response for the composite by homogenizing subcells in the thickness direction prior to homogenizing in-plane. This procedure was shown by Bednarcyk and Arnold (Ref. 7) to improve the prediction of in-plane properties and is typically used in conjunction with the MSGMC. This approach has been implemented within the NASA MAC/GMC code, (Ref. 8) and all calculations were performed using MAC/GMC.

Composite Structural Supercapacitor Concepts

In this study, the mechanical behavior of two composite supercapacitors, whose development and testing was recently reported in the literature, are investigated using MAC/GMC. Both supercapacitors are similar in construction with the main difference being the choice in separator material. These configurations are described in the following sections.

Concept 1: CF Electrodes/PP Separator

Snyder et al. (Ref. 2) developed a composite structural supercapacitor comprised of T300-3k plain weave carbon fiber electrodes, a 55 percent porous PP separator (Celgard 3501), and a vinyl ester (VE) SPE containing dissolved lithium bis(trifluoromethane-sulfonyl)imide (LiTFSI) salts. The SPE formulation had been previously optimized by Snyder et al. (Ref. 9) an RUC for the structural supercapacitor based on this concept was comprised of a plain weave fabric ply with a separator (Fig. 4(a)). The RUC was sized to give a 45 percent overall fiber volume fraction and 3.5 percent separator volume fraction, consistent with Snyder et al. (Ref. 2) the ply and separator thicknesses were 0.3 mm and 25 μm, respectively (Ref. 2). A 1.58 mm tow width (Ref. 10) was used in the simulations, and the tow was assumed to have an 80 percent fiber volume fraction. The T300 fiber was assumed to be transversely isotropic. Both isotropic elastic and inelastic material models were implemented for the VE/LiTFSI matrix. Since matrix material properties within the weave were unavailable, the matrix properties were calibrated in order to obtain the best fit of the experimental shear/tensile data. An isotropic elastic material model was used to represent the PP Celgard 3501 separator material. In order to approximate the porosity of the Celgard 3501 separator, a distinct, lower-Level RUC was generated (Fig. 4(b)). The separator was modeled as 45 percent Celgard 3501 with the 55 percent porosity filled with SPE matrix. This separator representation then is used as a layer in the higher scale model, which includes the CF weave representation (Fig. 4(a)). At each load increment, MSGMC homogenized this

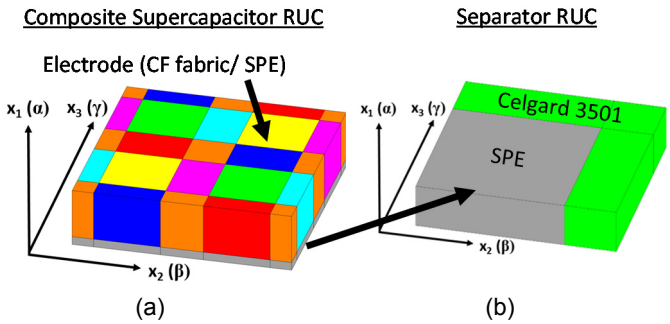

Figure 4.—MSGMC representation of (a) a T300-3k plain weave fabric electrode with an idealized Celgard 3501 separator and (b) a lower length scale used to represent the separator. The colors represent different materials on the global scale (equivalent to the numbered stacks in Fig. 3).

TABLE 1.—CONSTITUENT MATERIAL PROPERTIES FOR CONCEPT 1

Constituent	Property	Value	Source
T300	Axial Elastic Modulus	234.6 GPa	Yudhanto et al. (Ref. 15)
	Transverse Elastic Modulus	6.0 GPa	
	Axial Shear Modulus	18.2 GPa	
	Axial Poisson's Ratio	0.20	
	Transverse Poisson's Ratio	0.40	
SC15	Elastic Modulus	2.2 GPa	Justusson et al. (Ref. 11)
	Poisson's Ratio	0.36	
	Yield Strength	32.8 MPa	
VE/LiTFSI	Elastic Modulus	180 MPa	Correlation
	Poisson's Ratio	0.4	
	Yield Strength	6.5 MPa	
Celgard 3501	Elastic Modulus	1.3 GPa	Cannarella et al. (Ref. 16)
	Poisson's Ratio	0.4	

lower-Level RUC, and the homogenized response was passed to the global RUC analysis. The material parameters for each constituent are included in Table 1. Additionally, nonlinear material properties for the SC15 matrix (Applied Poleramic Inc.) were obtained from Justusson et al. (Ref. 11) and are shown in Table 1. Given these properties along with the T300 carbon fiber data, pure predictions can be made and compared with laminate shear and tensile test results provided by Snyder et al. (Ref. 2). For these simulations, the RUC was sized to give a 55 percent overall fiber volume fraction (Ref. 2).

An in-plane longitudinal strain was applied to the RUC in order to evaluate the tensile response of the composite consistent with ASTM D3039 (Ref. 12). In order to calculate the composite shear behavior, a more complicated procedure was implemented. ASTM D3518 (Ref. 13) is often used to determine experimentally the shear behavior of composites because of its simplicity. Using results from classical lamination theory, the in-plane shear behavior for a composite ply is inferred from tensile testing on a $[\pm 45]_s$ laminate. Numerically, a $[\pm 45]_s$ woven fabric laminate can be simulated by applying an equivalent set of loading conditions corresponding to a $[0]_s$ woven fabric laminate. This loading condition (normal/transverse stress, in-plane shear stress) can be derived from the composite stress transformation equations (Ref. 14). For a ply (with a local 1-2 coordinate system) oriented at some angle θ with respect to a global *x*-*y* coordinate system, the in-plane ply stresses (σ_1, σ_2, and τ_{12}), are related to the global normal/shear stresses (σ_x, σ_y, and τ_{xy}) by Equation (15),

$$\begin{Bmatrix} \sigma_x \\ \sigma_y \\ \tau_{xy} \end{Bmatrix} = \begin{bmatrix} \cos^2\theta & \sin^2\theta & -2\sin\theta\cos\theta \\ \sin^2\theta & \cos^2\theta & 2\sin\theta\cos\theta \\ \sin\theta\cos\theta & -\sin\theta\cos\theta & \cos^2\theta - \sin^2\theta \end{bmatrix} \begin{Bmatrix} \sigma_1 \\ \sigma_2 \\ \tau_{12} \end{Bmatrix} \tag{15}$$

Similarly, strain transformation equations can be derived by replacing the stress components in Equation (15) with the analogous tensorial strain components. By applying a stress in the global longitudinal (i.e., *x*-direction) direction consistent with a tensile test, the equivalent ply stresses σ_1, σ_2, and τ_{12}, can be calculated. These ply stresses were then applied to the global RUC (Fig. 4(a)). Note that, because of the choice of constitutive models for the matrix and separator material, the homogenized response of the separator is isotropic in-plane and unaffected by in-plane rotations. Hence the loading conditions applied to a single ply can be applied to the RUC. However, in order to calculate the shear stress-strain response from ASTM D3518, the longitudinal strain/stress and transverse strain with respect to the global coordinate system are required. These values were determined by substituting the appropriate ply stresses/strains into the previously mentioned stress/strain transformation equations. For laminates with arbitrary ply orientations, however, this approach would break down and a more complex modeling technique would be required.

Concept 2: CF Electrodes/E-Glass Fabric Separator

Qian et al. (Ref. 17) developed a similar composite structural supercapacitor to Concept 1. However, rather than using a PP separator, a plain weave E-glass fabric (TISSA Glasweberei AG) was used. The electrodes were an HTA-3k plain weave CF (TISSA Glasweberei AG). The SPE formulation consisted of a polyethylene glycol diglycidyl ether (PEGDGE)-based epoxy modified with an ionic liquid (IL). Four-ply laminates were fabricated using a resin infusion procedure by sandwiching two E-glass fabric plies between two CF plies. Since both the electrode and the separator are comprised of woven fabrics, each with its own weave geometry, generating a single RUC representative of the laminate is tedious. However, by defining an individual ply as a separate lower Level within MSGMC, a single global RUC comprised of one subcell for each ply can be easily generated. In addition, this approach facilitates the use of parametric studies by allowing the user to change any geometric properties of a woven fabric without increasing the complexity of the global RUC for the composite laminate. This procedure is graphically shown in Figure 5, where the woven electrode and woven separator were both represented at a lower scale and then combined as two layers at the global scale.

Qian et al. (Ref. 17) did not give an estimate of the fiber volume fraction for the E-glass and CF separately, but gave an estimate for the total fiber volume fraction (47.2 percent). The ratio of CF to E-glass was assumed to be 72:28 consistent with a previous study by the same research group for a similar composite (Ref. 4). A 0.3 mm thickness and 2.02 mm tow width was used for the plain weave CF fabric (Ref. 18). The plain weave E-glass fabric was simulated with a 0.16 mm thickness (Ref. 17) and 0.69 mm tow width (Ref. 19). Similar to Concept 1, the tow fiber volume fraction was assumed to be 80 percent for both the CF and E-glass plies. A transversely isotropic elastic material model was used for the HTA CF, and an isotropic elastic material model was used for the E-glass fiber and PEGDGE/IL matrix. Since material properties for the matrix were unavailable, the matrix properties were determined by calibrating the model to the experimental shear test data. The properties used in the simulations for Concept 2 are given in Table 2. It should be noted that Qian et al. (Ref. 17) also presented results for carbon aerogel reinforced composite structural supercapacitors. Although not considered as part of this study, the carbon aerogel structure could be represented as an additional Level within MSGMC. Similar loading conditions to Concept 1 were applied to the global RUC to determine the shear response of the composite supercapacitor.

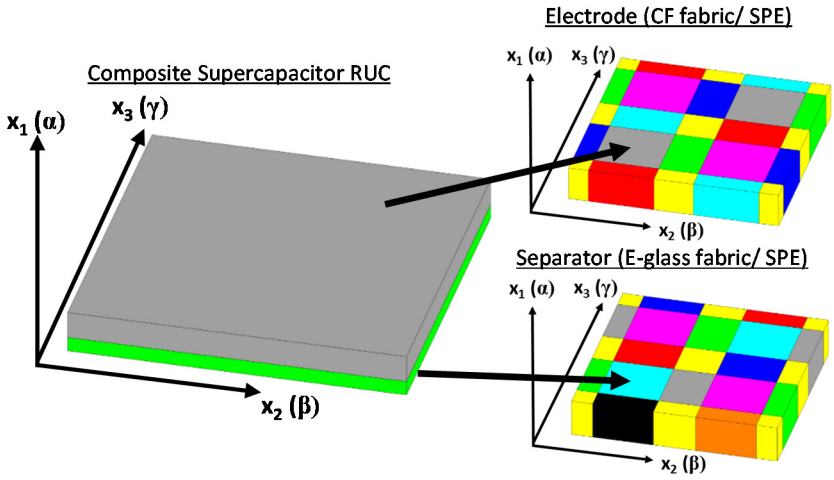

Figure 5.—MSGMC representation of an HTA-3k plain weave electrode with a plain weave E-glass fiber separator and the resulting composite supercapacitor RUC.

TABLE 2.—CONSTITUENT MATERIAL PROPERTIES FOR CONCEPT 2

Constituent	Property	Value	Source
HTA	Axial Elastic Modulus	238 GPa	Byström et al. (Ref. 20)
	Transverse Elastic Modulus	40 GPa	
	Axial Shear Modulus	22 GPa	
	Axial Poisson's Ratio	0.20	
	Transverse Poisson's Ratio	0.25	
E-glass	Elastic Modulus	73 GPa	Scida et al. (Ref. 21)
	Poisson's Ratio	0.2	
PEGDGE/IL	Elastic Modulus	230 MPa	Correlation
	Poisson's Ratio	0.4	

Results

The shear and tensile behavior of Concept 1 and the shear behavior of Concept 2 were simulated and compared to available experimental data from the literature (Refs. 2 and 17). Snyder et al. (Ref. 2) presented longitudinal stress-strain data based on a $[\pm 45]_s$ shear test and tensile stress-strain data for both the T300/SC15 and T300/VE/LiTFSI systems. The experimental and simulation data for the elastic shear and tensile behavior of Concept 1 are shown in Table 3. Since both constituents (T300 and SC15) have been relatively well characterized in the literature, the stress-strain behavior under tension and shear loading can be *predicted* to validate the current modeling approach. The error between the experimental and *predicted* elastic moduli was observed to be 12.3 percent for the tensile modulus and 6.1 percent for the slope of the $[\pm 45]_s$ stress-strain curve for the shear test. It should be noted that reported values for the elastic modulus of the SC15 matrix fall in the range 2.2 to 2.5 GPa (Ref. 11). Since the shear response of the composite is primarily driven by matrix properties, a 14 percent maximum increase in the elastic modulus of the SC15 matrix would likely improve the predicted shear response without significantly impacting the tensile behavior. Alternatively, since Snyder et al. (Ref. 2) did not provide any mechanical properties for the VE/LiTFSI matrix, optimal matrix properties were determined in order to minimize the error between simulation and experimental data (i.e., the simulations represent correlations). Based on this approach, the composite supercapacitor moduli were accurately correlated to within 12.3 percent. Provided experimental data were available for each constituent, the approach adopted in this study can likely be used for design purposes to predict composite supercapacitor elastic mechanical behavior.

The shear and tensile stress-strain behavior for both the composite supercapacitor (T300/VE/LiTFSI) and traditional composite (T300/SC15) are shown in Figure 6 where elastic constituent materials have been employed. The experimental shear and tensile stress-strain response of the composite supercapacitor was observed to be significantly lower than that of the traditional composite laminate. The difference in behavior is primarily attributed to the poor mechanical performance of current SPEs. Hence, a major area of ongoing research is aimed at maximizing both the mechanical and electrochemical performance of SPEs. Additionally, Snyder et al. (Ref. 2) noted an electrode/separator delamination for both shear and tensile composite supercapacitor specimens. The modeling approach developed in this study is primarily aimed at characterizing the *elastic* response of composite supercapacitors. A more sophisticated modeling approach would be required to simulate the delamination behavior. Since only elastic models were used to represent the constituents, the calculated composite shear response, shown in Figure 6, was never expected to capture any material nonlinearity. However in tension, the traditional composite laminate exhibited fairly linear stress-strain behavior and therefore the predicted stress-strain curve matches the experimental response reasonably well (Fig. 6(b)). The nonlinearity observed in the tensile stress-strain behavior for the composite supercapacitor is likely due to the onset of delamination rather than material nonlinearity.

TABLE 3.—SHEAR AND TENSILE RESULTS FOR CONCEPT 1

Material System	Shear-Slope of $[\pm 45]_s$ Stress-Strain Curve (MPa)		Error (%)	Tensile Modulus (MPa)		Error (%)
	Experiment	MSGMC		Experiment	MSGMC	
T300/SC15	10249	9625	–6.1	37694	42326	12.3
T300/VE/LiTFSI	738	798	8.1	16080	14097	–12.3

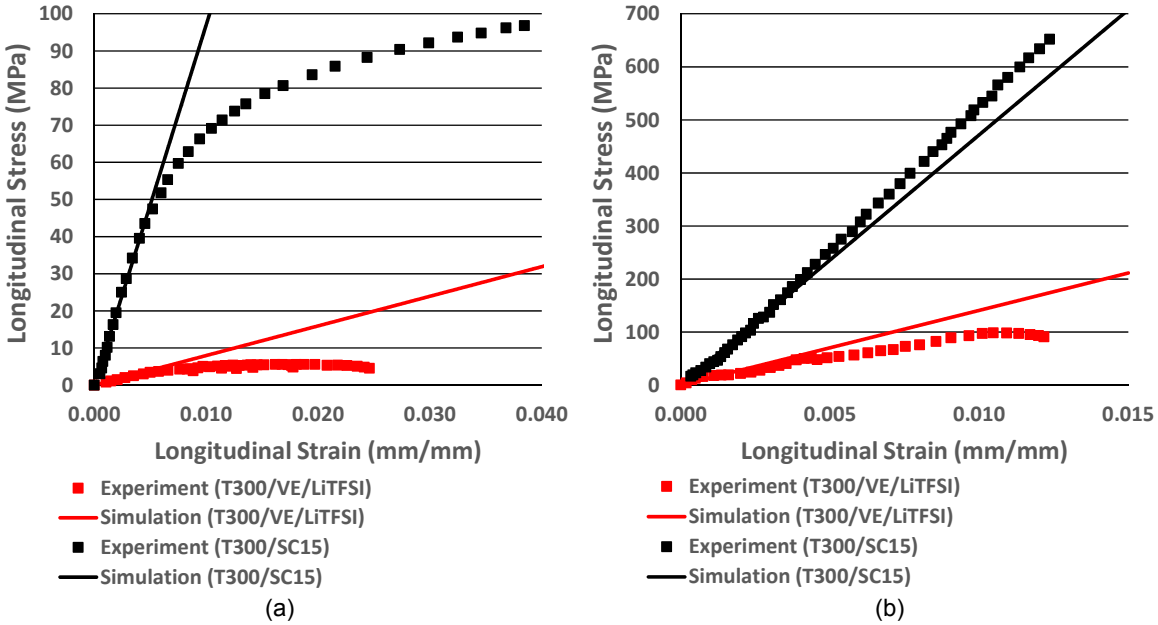

Figure 6.—Simulation a) $[\pm 45]_s$ shear and b) tensile stress-strain curves for Concept 1 and a traditional composite laminate compared to experimental data from Snyder et al. (Ref. 2) assuming elastic constituent properties.

A separate set of analyses was also performed where a rate-independent classical plasticity model was used to simulate the SC15 and VE/LiTFSI matrix. A multilinear plasticity model was fit to nonlinear SC15 stress-strain data (Ref. 11). The VE/LiTFSI matrix was assumed to be elastic-perfectly plastic and in the absence of experimental data, the yield stress was calculated so as to best match the composite shear behavior. Plots of the stress-strain responses for the $[\pm 45]_s$ shear and tensile tests of the supercapacitor and traditional laminate are shown in Figure 7. While the nonlinear behavior of both composites can be accurately captured in shear for small strains, the tensile behavior was not accurately calculated. Significant yielding was observed to occur within the tow at low mechanical loads in the simulation. This suggests that the classical plasticity approach adopted is incapable of simulating both ductile shear and brittle tensile behavior. A more sophisticated model that simulates damage rather than plastic flow would likely improve the simulations. Note, however, that the elastic properties are unchanged with this choice in nonlinear constitutive model for the matrix. Further, no attempt was made herein to model the interply behavior due to delamination.

Qian et al. (Ref. 17) presented experimental shear stress-strain data for Concept 2. Since Qian et al. (Ref. 17) did not provide experimental data on the PEGDGE/IL matrix, the matrix properties were calculated in order to match the experimental composite shear modulus (276 GPa). Unlike Concept 1, the experimental shear stress-strain response of Concept 2 exhibited fairly linear behavior as shown in Figure 8. As a result, an elastic matrix model was able to capture accurately the composite supercapacitor shear behavior. Using this approach, a shear modulus of 276.2 MPa was calculated which was within 0.1 percent of the experimentally reported value. Despite the general lack of constituent experimental data (particularly for the matrix), accurate micromechanical models can likely be generated to simulate composite structural supercapacitors.

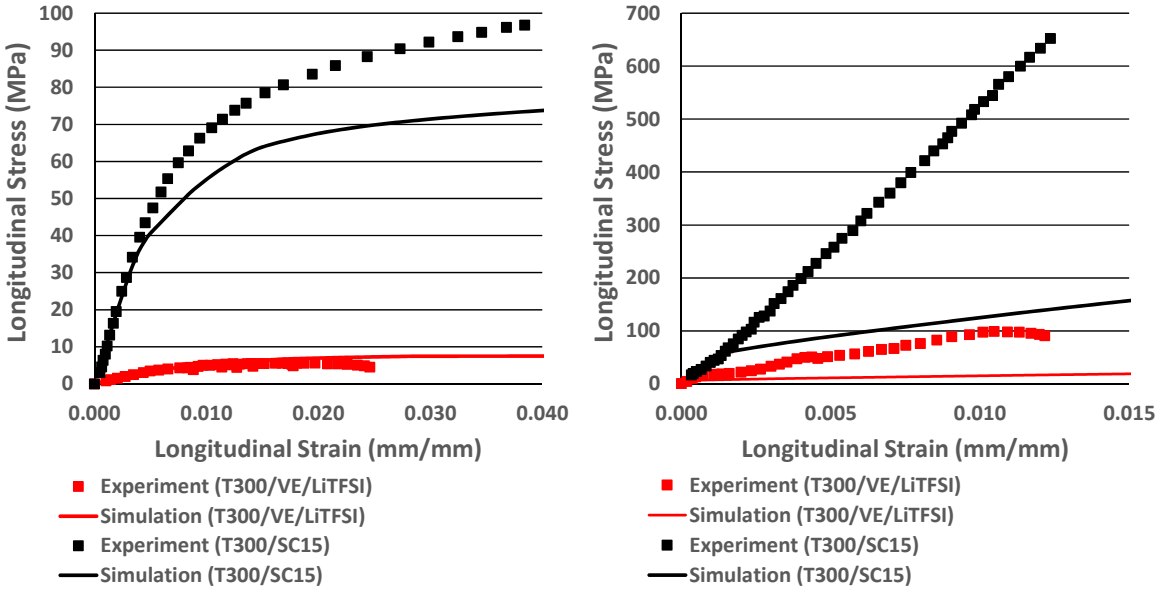

Figure 7.—Simulation a) $[\pm 45]_s$ shear and b) tensile stress-strain curves for Concept 1 and a traditional composite laminate compared to experimental data from Snyder et al. (Ref. 2) with a nonlinear matrix modeled with classical plasticity.

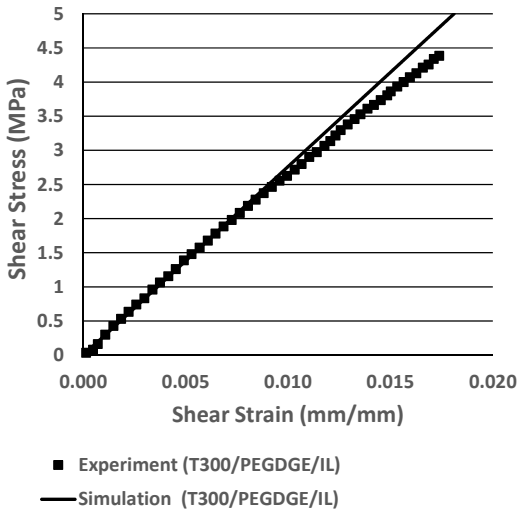

Figure 8.—Simulation of the shear stress-shear strain response for Concept 2 compared to experimental data from Qian et al. (Ref. 17).

Conclusions

In this study, mechanical models based on the Multiscale Generalized Method of Cells (MSGMC) were developed and used to calculate the shear and tensile response of two composite structural supercapacitor concepts from the literature. Both concepts were comprised of plain weave carbon fabric electrodes infused with a structural polymer electrolyte. The separator material was either a porous polypropylene membrane or a plain weave E-glass fabric. A preliminary simulation of a traditional composite laminate validated the adopted MSGMC modeling approach. Subsequent shear and tensile simulations for the two composite supercapacitor concepts demonstrated that accurate estimates of the composite elastic behavior can be obtained from the developed models. The approach developed in this work can be readily adapted to simulate other composite material systems. Ongoing work is aimed at improving the predictive capability of the MSGMC models.

References

1. Asp, L. E., and Greenhalgh, E. S., "Structural Power Composites," *Composites Science and Technology*, Vol. 101, 2014, pp. 41-61.
2. Snyder, J. F., Gienger, E. B., and Wetzel, E. D., (2015). "Performance Metrics for Structural Composites with Electrochemical Multifunctionality," *Journal of Composite Materials*, Vol. 49, No. 15, 2015, pp. 1-14.
3. Todoroki, A., Shiomi, H., Mizutani, Y., and Suzuki, Y., "Electrical Shorting Between the Carbon-Fiber Cloth Electrodes of Structural Capacitors With a Glass-Fiber Cloth Separator," *Open Journal of Composite Materials*, vol. 4, 2014, pp. 140–147.
4. Shirshova, N., Qian, H., Shaffer, M.S., Steinke, J.H., Greenhalgh, E.S., Curtis, P.T., Kucernak, A., and Bismarck, A., "Structural Composite Supercapacitors," *Composites: Part A*, Vol. 46, 2013, pp. 96–107.
5. Liu, K.C., Chattopadhyay, A., Bednarcyk, B.A., and Arnold, S.M., "Efficient Multiscale Modeling Framework for Triaxially Braided Composites using Generalized Method of Cells," *Journal of Aerospace Engineering*, vol. 24, 2011, pp. 162–169.
6. Aboudi, J., Arnold, S.M., and Bednarcyk, B.A., *Micromechanics of Composite Materials*, Elsevier, Oxford, UK, 2013, Ch. 5.
7. Bednarcyk, B.A., and Arnold, S.M., "Micromechanics-Based Modeling of Woven Polymer Matrix Composites," *AIAA Journal*, vol. 41, no. 9, 2003, pp. 1788–1796.
8. Bednarcyk, B.A., and Arnold, S.M., "MAC/GMC 4.0 User's Manual - Keywords Manual," NASA Glenn Research Center, NASA/TM—2002-212077/VOL2, Cleveland, OH, Dec. 2002.
9. Snyder, J.F., Carter, R.H., and Wetzel, E.D., "Electrochemical and Mechanical Behavior in Mechanically Robust Solid Polymer Electrolytes for Use in Multifunctional Structural Batteries," *Chemistry of Materials*, vol. 19, no. 15, 2007, pp. 3793–3801.
10. De Carvalho, N.V., Pinho, S.T., and Robinson, P., "Analytical Modeling of the Compressive and Tensile Response of Woven Composites," *Composite Structures*, vol. 94, no. 9, 2012, pp. 2724–2735.
11. Justusson, B., Yu, J., Chen, A., and Yen, C.-F., "Mechanical Testing of 3D Fabric Composites and Their Matrix Material SC-15," U.S. Army Research Laboratory, Rept. ARL-TR-6245, Aberdeen Proving Ground, MD, Nov. 2012.
12. ASTM D3039/D3039M-14, "Standard Test Method for Tensile Properties of Polymer Matrix Composite Materials," ASTM International, 2014.
13. ASTM D3518/D3518M-13, "Standard Test Method for In-Plane Shear Response of Polymer Matrix Composite Materials by Tensile Test of a ±45° Laminate," ASTM International, 2013.
14. Jones, R.M., *Mechanics of Composite Materials*, 2nd ed., Taylor & Francis, Philadelphia, 1999, p. 74.
15. Yudhanto, A., Iwahori, Y., Watanabe, N., and Hoshi, H., "Open hole fatigue characteristics and damage growth of stitched plain weave carbon/epoxy laminates," *International Journal of Fatigue*, vol. 43, 2012, pp. 12–22.

16. Cannarella, J., Liu, X., Leng, C.Z., Sinko, P.D., Gor, G.Y., and Arnold, C.B., "Mechanical Properties of a Battery Separator under Compression and Tension," *Journal of the Electrochemical Society*, vol. 161, no. 11, 2014, pp. 3117–3122.
17. Qian, H., Kucernak, A. R., Greenhalgh, E.S., Bismarck, A., and Shaffer, M.S., "Multifunctional Structural Supercapacitor Composites Based on Carbon Aerogel Modified High Performance Carbon Fiber Fabric," *ACS Applied Materials & Interfaces*, vol. 5, 2013, pp. 6113–6122.
18. TISSA Glasweberei AG, "technical datasheet," Product Number: 862.0200.01.1000, 2016.
19. TISSA Glasweberei AG, "technical datasheet," Product Number: 842.0200.01.1110, 2016.
20. Byström, J., Jekabsons, N., and Varna, J., "An evaluation of different models for prediction of elastic properties of woven composites," *Composites: Part B*, Vol. 31, 2000, pp. 7–20.
21. Scida, D., Aboura, Z., Benzeggagh, M.L., and Bocherens, E., "A micromechanics model for 3D elasticity and failure of woven-fibre composite materials," *Composites Science and Technology*, vol. 59, 1999, pp. 505–517.